JOURNAL OF COMPUTATIONAL PHYSICS 58, 44–58 (1985)

A Noise Suppression Algorithm for the Numerical Solution of Maxwell's Equations

M. CHAPMAN AND E. M. WAISMAN

S-CUBED, P. O. Box 1620, La Jolla, California 92038

Received October 4, 1983; revised February 2, 1984

A grid noise suppression algorithm for the numerical solution of Maxwell's equations is developed. The algorithm introduces nonlinear diffusive damping into the equations governing the transverse components of the electromagnetic fields. The transverse-longitudinal field decomposition is preserved by the damping; however, the energy in short wavelengths associated with the grid size is dissipated, and therefore total energy is not conserved. Examples are given of one- and two-dimensional vacuum wave propagation and a one-dimensional planar relativistic diode. In particular, it is shown for the case of one-dimensional vacuum wave propagation that this technique reduces the computational errors as compared to leapfrog in the L_1, L_2, and L_∞ norms. © 1985 Academic Press, Inc.

INTRODUCTION

We describe in this article the generalization of Filtering Remedy and Metholodogy (FRAM) [1] to the numerical solution of Maxwell's equations. This technique is introduced to reduce grid noise, that is, the noise of wavelengths associated with the grid size of the discrete mesh used to solve the equations. Even in pure electromagnetic (em) wave propagation in vacuum, or other homogeneous media, this short wavelength noise is significant if one considers sharp wave packets. In the case of em propagation in vacuum the equations are linear in the fields and post-filtering techniques can be used. That is not the case in the presence of particle-electron and ions-currents, which become nonlinear sources in Maxwell's equations. The grid noise couples, therefore, in a nonlinear fashion and post-filtering of the unphysical numerical noise might become inappropriate.

We envision the applications of this technique, as a significant improvement over the traditional leapfrog method, to cases in which Maxwell's equations become nonlinear. Illustrative examples are: Wave propagation in nonlinear media and electromagnetic and plasma particle simulations. This technique is also a viable alternative to post-filtering in the numerical solution of sharp wave packet propagation even when the equations are linear.

The organization of this article is as follows:

(a) introduction of FRAM as generalized for E and M;

0021-9991/85 $3.00

Copyright © 1985 by Academic Press, Inc.
All rights of reproduction in any form reserved.

(b) application to 1–D and 2–D vacuum wave propagation;

(c) application to a 1–D relativistic electron diode;

(d) conclusions.

a. Introduction of FRAM as Generalized for E and M

We consider Maxwell's equations in the form in which the vector quantities are the sum of the transverse, divergence free, and longitudinal, curl-free, components. For the transverse components we have

$$c\nabla \times \mathbf{E}_\mathrm{T} = -\partial \mathbf{B}/\partial t; \qquad c\nabla \times \mathbf{B} = \partial \mathbf{E}_\mathrm{T}/\partial t + 4\pi \mathbf{J}_\mathrm{T}; \qquad \nabla \cdot \mathbf{E}_\mathrm{T} = \nabla \cdot \mathbf{B} = 0. \tag{1}$$

The transverse part of the current density $\mathbf{J}_\mathrm{T}$ is given by $\mathbf{J}_\mathrm{T} = \mathbf{J} + (1/4\pi)(\partial/\partial t)\,\mathbf{E}_\mathrm{L}$. In this expression $\mathbf{J}$ is the total current density and $\mathbf{E}_\mathrm{L}$ is the longitudinal part of the electric field and satisfies Poisson's equation $\nabla \cdot \mathbf{E}_\mathrm{L} = 4\pi\rho$, where ρ is the charge density. Naturally $\mathbf{B}$ is purely transverse.

A widely used algorithm to solve Eqs. (1) is leapfrog [2]. To reduce the grid noise generated by leapfrog we introduce the following modified set of equations:

$$\mathbf{E}_\mathrm{T}^{n+1} = \tilde{\mathbf{E}}_\mathrm{T}^{n+1} - \nabla \times \alpha_E \nabla \times \mathbf{E}_\mathrm{T}^{n}\,\Delta t, \tag{2a}$$

$$\mathbf{B}^{n+1/2} = \tilde{\mathbf{B}}^{n+1/2} - \nabla \times \alpha_B(\nabla \times \mathbf{B}^{n-1/2} - 4\pi \mathbf{J}_\mathrm{T}^{n-1/2}/c)\,\Delta t. \tag{2b}$$

In Eqs. (2) $\tilde{\mathbf{E}}_\mathrm{T}$ and $\tilde{\mathbf{B}}$ stand for the leapfrog solution of Eqs. (1) obtained at the $(n+1)$th timestep of integration from the complete algorithm solution at the nth timestep.

In Eqs. (2a) and (2b) the diffusive correction must be constructed by using the previous timestep fields for the algorithm to be monotonic [3]. It is this feature that assures the suppression of spurious nonphysical oscillations. The quantities α_E and α_B are nonlinear anisotropic numerical diffusivities which are functions of space and time and are zero in regions of smooth solutions of the leapfrog equations and nonzero, in a manner and value that we discuss below, in regions for which leapfrog produces nonphysical oscillations.

The form of the added terms in Eqs. (2) are such that

(i) the second spatial order operators are diffusion-like terms, and in the linear sense when α_E and $\alpha_B \neq 0$ they produce dissipative terms of order k^2 in Fourier space;

(ii) the algorithm reproduces the solution to Maxwell's continuum equations for long wavelengths: long compared with the mesh spacing;

(iii) by their form they preserve the transverse nature of $\mathbf{E}_\mathrm{T}$ and $\mathbf{B}$.

We turn our attention now to the central point of how to choose the functions α_E

and α_B as to realize an accurate representation of the solution of Maxwell's equations.

A truncation error analysis of the leapfrog algorithm shows that it is second order accurate in space and time for uniform grid spacing. The leading order error term contains third order derivatives in each of the coupled equations. The addition in Eqs. (2) of second order space operators is therefore added to make the algorithm monotonic in the sense of Reference 4. The diffusivities α_E and α_B are then obtained by using the Taylor remainder theorem, i.e., by choosing them as to be greater than the remainder of the truncation error of the leapfrog algorithm. For the one-dimensional wave propagation in vacuum in an equally space mesh, one obtains $\alpha_E = \alpha_B = c(\Delta x/2 - c\,\Delta t/2)$. The diffusion-like terms in Eq. (2), which are energy dissipative in nature, formally reduce the difference scheme to first order in space in time.

To avoid unneeded diffusion, and dissipation, α_E and α_B are switched to nonzero values only if the numerical solution exceeds local physical bounds. Since the leapfrog algorithm is explicit in time, wave information cannot cross a full mesh increment in one timestep and physical bounds are obtained, for instance, by estimating the local characteristic solutions obtained at time n from the nearest neighbor information of a given cell. We find that less stringent upper and lower bounds, like the maximum and minimum of the fields at neighboring points, are adequate in that they produce accurate answers as we shall see from our 2–D example.

In summary, Eqs. (2) are used with the following prescription (e.g., for α_E and one of the components of $\mathbf{E}_\mathrm{T}$):

$$\begin{aligned} &\alpha_E = 0 && \text{if } E^*_{\min} < \tilde{E} < E^*_{\max}, \qquad (3)\\ &\alpha_E \simeq \left(c\,\Delta l/2 - c^2 \frac{\Delta t}{2}\right) && \text{otherwise,} \end{aligned}$$

where Δl is Δx in 1–D and a typical mesh spacing length in higher dimensions and $E^*_{\min}$ and $E^*_{\max}$ represent the physical bounds described above.

To conclude this part, let us remark that the operations needed to suppress noise in $\mathbf{E}_\mathrm{T}$, $\mathbf{B}$ are a very small fraction of the time used in the typical "pushing" of particles in E & M plus particle simulations.

b. 1–D and 2–D Vacuum Wave Propagation

We consider the propagation in vacuum in the X direction of a 1–D wave with $\mathbf{B} = B\hat{z}$ and $\mathbf{E} = E\hat{y}$. We use an equally spaced mesh and drop the subindexes T and L, because in this and the following example the fields are purely transverse. The time and space centering is represented by the notation E^n_j, $B^{n+1/2}_{j+1/2}$, where the superscript represents time level and the subscript mesh location. Any values of E

or B not centered in this way are to be interpreted as the corresponding arithmetic means over neighboring points and time levels, for instance,

$$E^{n-1/2}_{j-1/2} = 1/4[E^n_j + E^n_{j+1} + E^{n+1}_j + E^{n+1}_{j+1}]. \tag{4}$$

We define a switch function associated with field components F as

$$\delta F = \begin{cases} 0 & \text{if} \quad F_{\text{MIN}} \leqslant \tilde{F} \leqslant \text{F}_{\text{MAX}}, \\ 1 & \text{otherwise,} \end{cases} \tag{5}$$

where $\tilde{F}$ is the provisional value of F advanced from the full solution of the previous timestep by leapfrog and F_{MIN} and F_{MAX} are physical bounds on F as explained in *a*.

For this example it is advantageous to define the forward and backwards local characteristics, i.e.,

$$G^{\pm} = E \mp B. \tag{6}$$

Having introduced the necessary notation we now write the difference equations for B and E, i.e.,

$$\begin{aligned} B^{n+1/2}_{j+1/2} = \tilde{B}^{n+1/2}_{j+1/2} &+ (\Delta t/\Delta x^2)[\alpha_{j+1}(B^{n-1/2}_{j+3/2} - B^{n-1/2}_{j+1/2}) \\ &- \alpha_j(B^{n-1/2}_{j+1/2} - B^{n-1/2}_{j-1/2})], \end{aligned} \tag{7}$$

where

$$\alpha_j = 1/2(c\,\Delta x - c^2\,\Delta t)\,\text{Max}[\delta B^{n-1/2}_{j+1/2}, \delta B^{n-1/2}_{j-1/2}, \delta E^n_j]. \tag{8}$$

In Eqs. (7) and (8) and in what follows we use α to denote either α_E or α_B. In the evaluation of the δB switches of Eq. (8) the values employed for B_{MAX} and B_{MIN} are, for instance, for $\delta B^{n-1/2}_{j+1/2}$,

$$[\text{M, m}]\, B^{n-1/2}_{j+1/2} = [\text{M, m}][B^{*n-1/2}_{j+1/2}, B^{n-1/2}_{j+1/2}], \tag{9}$$

where [M, m] represents the Max and Min respectively, and

$$B^{*n-1/2}_{j+1/2} = (1/2)[G^{-n-1/2}_{j+3/2} - G^{+n-1/2}_{j-1/2}]. \tag{10}$$

The switch δE^n_j in Eq. (8) comes from the n time update for E. The difference equation used to advance E is

$$E^{n+1}_j = \tilde{E}^{n+1}_j + (\Delta t/\Delta x^2)[\alpha_{j+1/2}(E^n_{j+1} - E^n_j) - \alpha_{j-1/2}(E^n_j - E^n_{j-1})], \tag{11}$$

where

$$\alpha_{j+1/2} = 1/2(c\,\Delta x - c^2\,\Delta t)\,\text{Max}[\delta E^n_j, \delta E^n_{j+1}, \delta B^{n+1/2}_{j+1/2}], \tag{12}$$

TABLE I

	L_1	L_2	L_∞
FRAM plus leapfrog	7.8	3.6	0.98
Leapfrog	14.4	6.11	1.28
Damped	20.5	12.1	0.98

and in the evaluation for the δE switches in Eq. (12), the bounds used are, for instance, for δE_j^n,

$$[\mathrm{M}, \mathrm{m}]\, E_j^n = [\mathrm{M}, \mathrm{m}][E^{*n}_j, E_j^n] \tag{13}$$

where

$$E^{*n}_j = (1/2)[G^{+n}_{j-1} + G^{-n}_{j+1}]. \tag{14}$$

The above algorithm was tested on a long wavelength standing wave $\lambda = 200\,\Delta x$ for one period and the results were identical to machine roundoff with leapfrog alone. The other test problem was propagation of a square pulse 20 cells wide through a uniform mesh of $\Delta x = 1$, $c\,\Delta t/\Delta x = 1/3$ for 120 timesteps.

Figure 1 shows the results for the FRAM algorithm, pure leap frog and the case in which the numerical diffusion is always on. Table I shows computed error for cases (1)–(3), where the notation L_1, L_2, L_∞ refers to the absolute value norm, the square norm and the supremum norm, respectively.

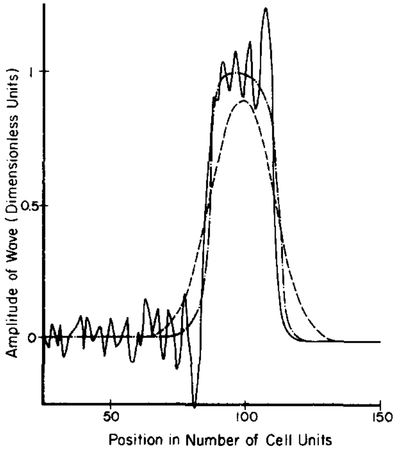

FIG. 1. Square wave of 20 cells wide propagating through a 1-D equally space mesh after 120 timesteps for $c\,\Delta t/\Delta x = \frac{1}{3}$ with periodic boundary conditions; Leapfrog (—), FRAM (-·-), pure diffusion (——).

We now turn our attention to a 2–D Cartesian example with field components E_x, E_y, B_z. The differential equations, as modified by the numerical diffusion terms are

$$\partial E_x/\partial t = -c\,\partial B_z/\partial y + \partial/\partial x\,(\alpha_{1x}\,\partial E_x/\partial x) + \partial/\partial y\,(\alpha_{1y}\,\partial E_x/\partial y), \tag{15a}$$

$$\partial E_y/\partial t = c\,\partial B_z/\partial x + \partial/\partial x\,(\alpha_{2x}\,\partial E_y/\partial x) + \partial/\partial y\,(\alpha_{2y}\,\partial E_y/\partial y), \tag{15b}$$

$$\partial B_z/\partial t = c\left(\frac{\partial E_y}{\partial x} - \frac{\partial E_x}{\partial y}\right) + \partial/\partial x\,(\alpha_{3x}\,\partial B_z/\partial x) + \partial/\partial y\,(\alpha_{3y}\,\partial B_z/\partial y). \tag{15c}$$

In Eqs. (15) α_{ix}, α_{iy}, α_{iz} denote the diffusivities in the x, y, z directions corresponding to field component i, with the assignment $i=1$ to E_x, $i=2$ to E_y, and $i=3$ to B_z. We use an equally space mesh $\Delta x = \Delta y = \Delta$ and the field centering used is shown in Fig. 2. For the sake of brevity we give the difference equation to advance E_x: the ones for E_y and B_z are completely equivalent up to centering and the reader can obtain them in a straightforward manner. To avoid carrying too many subindexes we use E for E_x and B for B_z, we then have

$$\begin{aligned} E^{n+1/2}_{i+1/2,j} = \tilde{E}^{n+1/2}_{i+1/2,j} + \Delta t\,(&[F^{n-1/2}_{i+1,j} - F^{n-1/2}_{i,j}]/\Delta x \\ &+ [F^{n-1/2}_{i+1/2,j+1/2} - F^{n-1/2}_{i+1/2,j-1/2}]/\Delta y), \end{aligned} \tag{16}$$

where the numerical diffusion fluxes are given by

$$F^{n-1/2}_{i+1,j} = \alpha_{1x}(E^{n-1/2}_{i+3/2,j} - E^{n-1/2}_{i+1/2,j})/\Delta x, \tag{17a}$$

$$F^{n-1/2}_{i+1/2,j+1/2} = \alpha_{1y}(E^{n-1/2}_{i+1/2,j+1} - E^{n-1/2}_{i+1/2,j})/\Delta y, \tag{17b}$$

where α_{1x} and α_{1y}, at $i+1, j$ and $i+1/2, j+1/2$, respectively, are given by

$$\alpha_{1x} = 1/2(c\,\Delta x - c^2\,\Delta t)\,\mathrm{Max}[\delta E^{n-1/2}_{i+3/2,j}, \delta E^{n-1/2}_{i+1/2,j}, \delta B^{n}_{i+1,j}], \tag{18a}$$

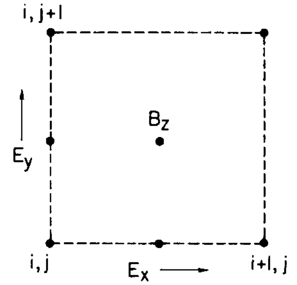

FIG. 2. Centering of fields used in two-dimensional vacuum wave propagation.

where

$$\delta B^n_{i+1,j} = \mathrm{Max}[\delta B^n_{i+1/2,j+1/2}, \delta B^n_{i+3/2,j+1/2}, \delta B^n_{i+1/2,j-1/2}, \delta B^n_{i+3/2,j-1/2}], \quad (18b)$$

$$\alpha_{1y} = 1/2(c\,\Delta x - c^2\,\Delta t)\,\mathrm{Max}[\delta E^{n-1/2}_{i+1/2,j+1}, \delta E^{n-1/2}_{i+1/2,j}, \delta B^{n+1/2}_{i,j}]. \quad (18c)$$

Note in Eqs. (18a), (18b), and (18c) that the centering of switch δB is not completely compatible with the other quantities; this is done to keep the algorithm simple, and we find that this does not detract from our results.

The bounds used to evaluate the switches in Eqs. (18a) and (18b) are, for instance, for $E^{n-1/2}_{i+1/2,j}$,

$$[\mathrm{M}, \mathrm{m}]\, E^{n-1/2}_{i+1/2,j} = [\mathrm{M}, \mathrm{m}][E^{n-1/2}_{i+1/2,j}, E^{n-1/2}_{i+3/2,j}, E^{n-1/2}_{i-1/2,j}, E^{n-1/2}_{i+1/2,j+1}, E^{n-1/2}_{i+1/2,j-1}], \quad (19)$$

that is, the Max or Min of the field component at its own location and its four nearest neighbors. The definition for $[\mathrm{M}, \mathrm{m}]\, B^n_{i,j}$ follows exactly the same lines.

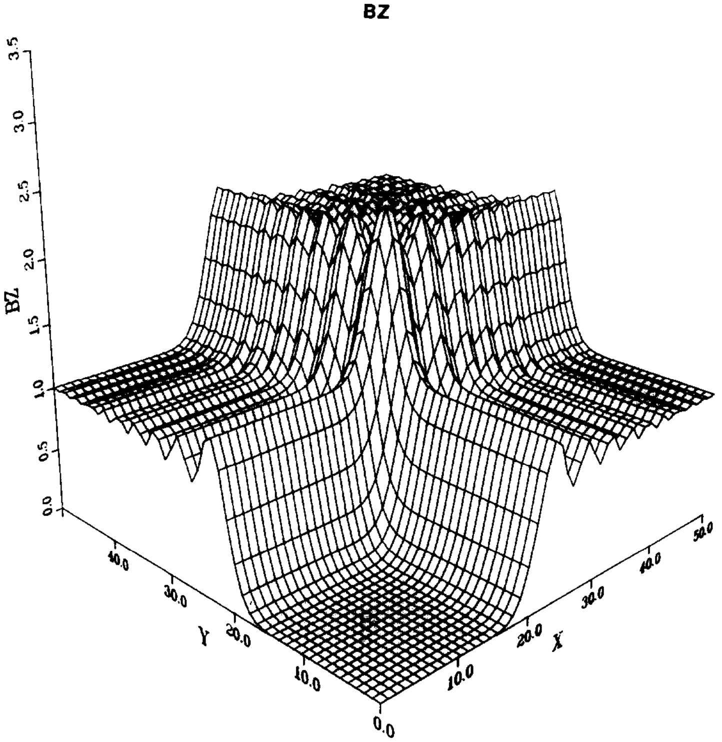

FIG. 3. Magnetic field versus x, y for leapfrog for two-dimensional wave propagation in vacuum at $t = 90\,\Delta t$.

This algorithm has been coded and tested on the following test problem:

$$Ex = Ey = Bz(x, y, 0) = 0,$$

$$Ey(x = 50, y, t) = -1,$$

$$Ex(x, y = 50, t) = 1,$$

$$\Delta x = \Delta y = 1, \; c\,\Delta t/\Delta x = 1/3.$$

Figures 3–8 show the results of three test calculations at $t = 90\,\Delta t$. We plot the B_z field in Figs. 3–5 and in Figs. 6–8 the field energy density, i.e., $|\mathbf{E}|^2 + |\mathbf{B}|^2$. Figures 3 and 6 are the results of the basic leapfrog algorithm and as expected the quantities plotted are quite noisy behind the wavefronts. Figures 4, 7 show the results with $\delta B = \delta E = 1$ for all x, y, t, that is, the dissipation on always. Note the noise is suppressed but the wavefronts are quite diffuse. Figures 5 and 8 show the results of the complete algorithm. Note the sharp fronts with the suppression of grid noise.

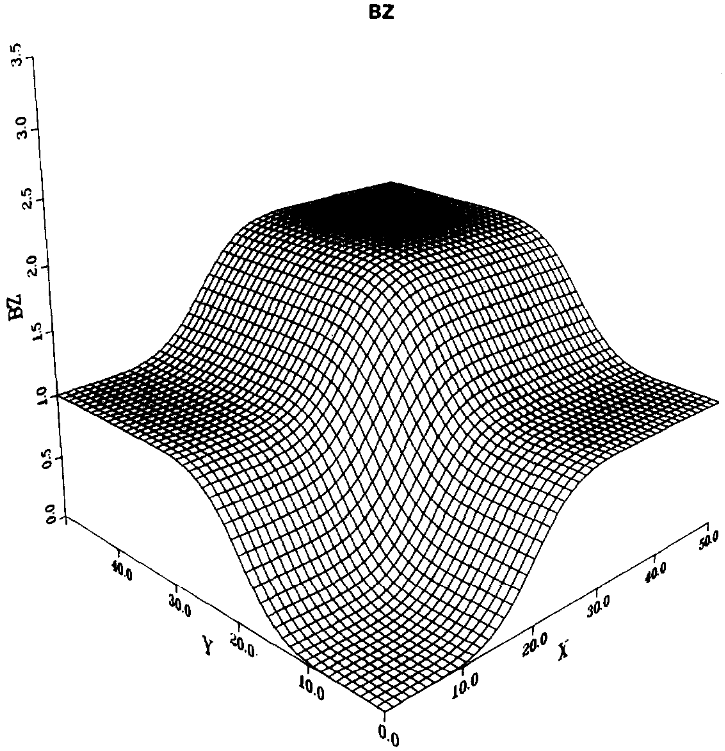

FIG. 4. Same as Fig. 3 but leapfrog → diffusive algorithm.

c. 1-D Planar Relativistic Diode in a Magnetic Field

We show here an example of how numerical diffusion applied to the transverse part of the em fields can be used to accelerate and stabilize convergence in calculations that use relaxation pseudo-time marching procedures to obtain a steady-state solution for a given system.

To this end let us consider a 1-D planar relativistic diode with an applied voltage V between the anode and cathode plates located at $y=d$ and $y=0$, respectively. A magnetic field in the z direction B_z is present, such that the flux per unit length in the x direction $\psi=\int_0^d B_z\,dy$ is time conserved. Electrons start at the cathode surface with velocity $\mathbf{v}=0$ and their emission current is space-charge limited. Electron trajectories stay in the x, y plane, the field components present E_x, E_y, and B_z are only functions of y and t.

The differential equations satisfied by the fields are

$$\partial E_y/\partial y = -\partial^2\phi/\partial y^2 = 4\pi\rho, \tag{20a}$$

$$\partial E_x/\partial t = c\,\partial B_z/\partial y - 4\pi J_x, \tag{20b}$$

$$\partial B_z/\partial t = c\,\partial E_x/\partial y, \tag{20c}$$

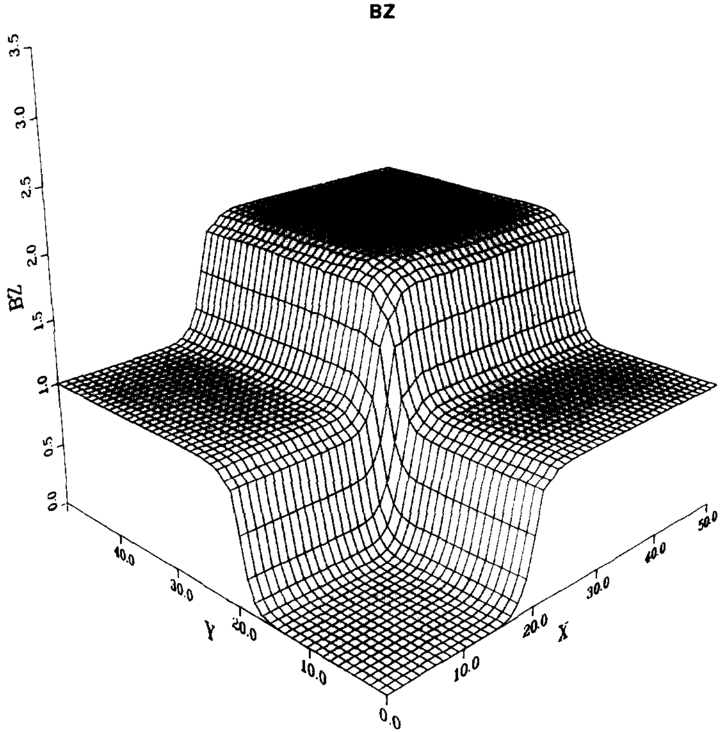

Fig. 5. Same as Fig. 3 but leapfrog → FRAM.

where we have introduced in Eq. (20a) the electric potential ϕ and ρ is the charge density.

The boundary conditions (bc) are

$$\phi(0)=0, \tag{21a}$$

$$\phi(d)=-\int_0^d E_y\,dy=V, \tag{21b}$$

$$E_y(0)=0, \tag{21c}$$

$$E_x(d)=E_x(0)=0. \tag{21d}$$

We observe that integrating Eq. (20c) in y and using the metallic (bc) of Eq. (21d) for E_x, one obtains that $\partial/\partial t \int_0^d B_z\,dy=0$. The bc of Eq. (21a) is the statement of space-charge limited emission. Equations (21a), (21b), and (21c) together are (bc) for the solution of Poisson's equation (20a) and determine the electron emission current density as a function of time. The electron dynamics is given by

$$d\mathbf{p}/dt=-e(\mathbf{E}+\mathbf{v}\times\mathbf{B}), \tag{22}$$

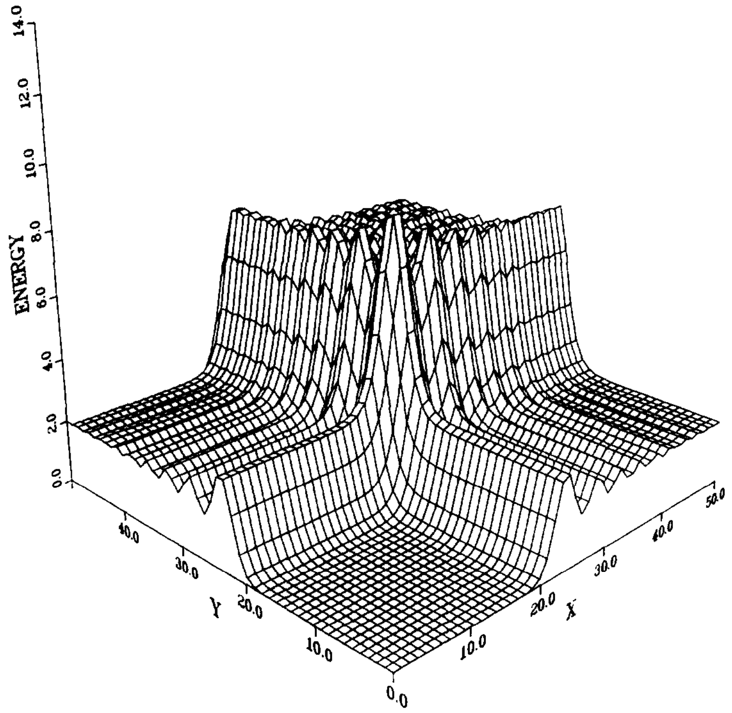

FIG. 6. Field energy. Same as Fig. 3 but magnetic field → field energy density.

where $\mathbf{p} = m_0\gamma\mathbf{v}$, with m_0 being the electron rest mass and $\gamma = 1/\sqrt{1-(v/c)^2}$. The electron current is given by $\mathbf{J} = \rho\mathbf{v}$. An interesting property of the 1–D diode set of equations is that E_y^{T} and E_x^{L} are constant in y and can be taken to be zero without any loss of generality. That results in $J_x^{\mathrm{T}} = J_x$.

To obtain steady state, that is a state in which $E_x(y, t) = 0$ and B_z and E_y have time independent self-consistent profiles, we initialize the problem with zero charge in the gap and

$$B_z(y, 0) = \psi/d, \tag{23a}$$

$$E_x(y, 0) = 0. \tag{23b}$$

The potential at the anode $\phi(d)$ is linearly ramped from zero to the value $\phi(d) = V$ in about two cyclotron periods, $\tau_c = 2\pi m_0 cd/\psi$. The calculation is continued thereafter keeping that constant value V for $\phi(d)$ for a few more τ_c's. In our calculations, we considered a case for which $e\psi/(m_0c^2) < \sqrt{(1+eV/m_0c^2)^2 - 1}$ for which a steady state exists such that the emitted electrons cross the gap [5].

The numerical example we report is with $V = 1$ MV, $\psi = 3$ kGcm, $d = 1$ cm. We used a 25-zone uniform grid. In each timestep Poisson's equation is solved, the emission current is calculated and the field is advanced; electrons are pushed using

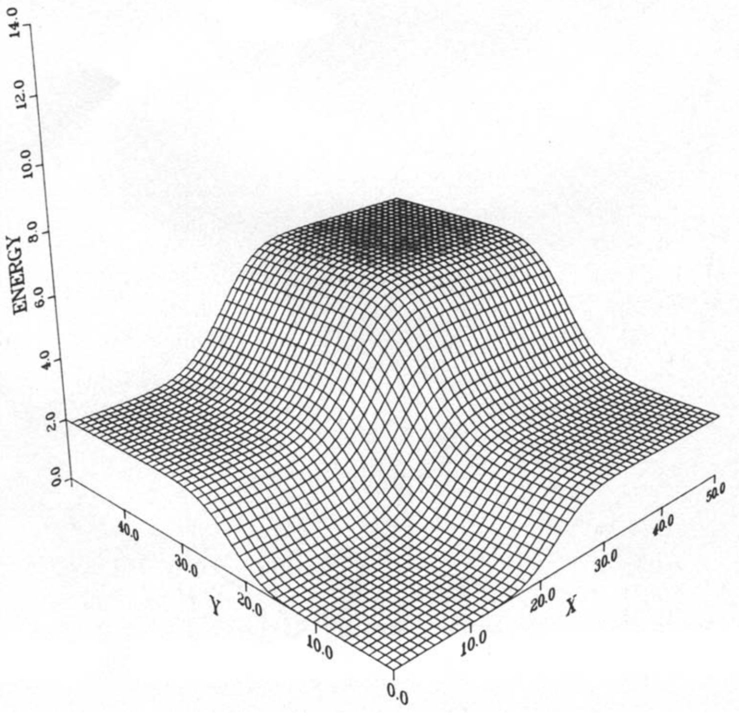

FIG. 7. Field energy. Same as Fig. 6 but diffusive algorithm.

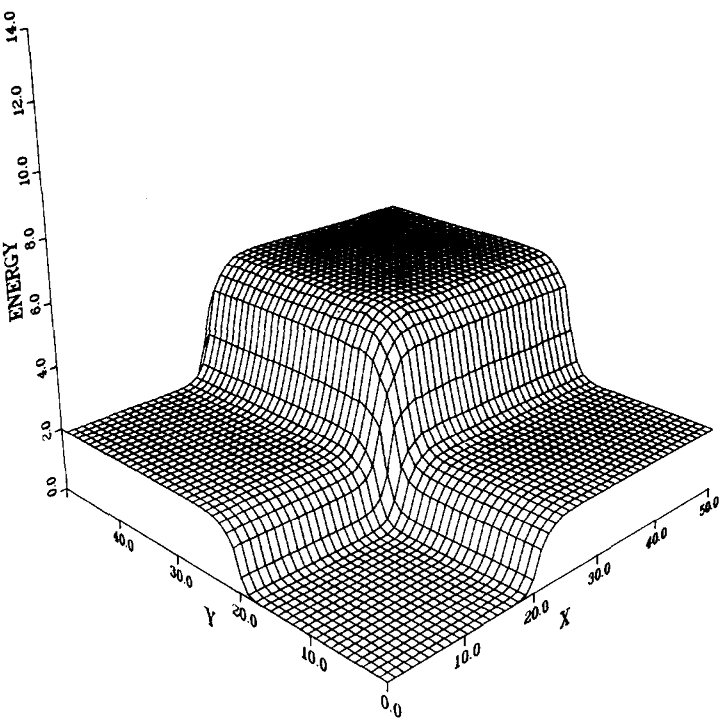

FIG. 8. Field energy. Same as Fig. 6 but with FRAM.

a time-centered relativistic algorithm [2]. Charge and current are shared in the grid using particles in cell linear interpolation.

The pair of Maxwell's equations (20b) and (20c) is solved using the algorithm described in the 1–D vacuum case with two important differences: (i) as written in Eq. (2b) the diffusive flux for the B field equation contains the current; i.e., $\nabla \times \mathbf{B} - 4\pi \mathbf{J}_T/c$ and (ii) the diffusivities α_E and α_B were constant in time and space and set equal to 2c Δy.[1] The diffusivities are selected in this way because as we have stated at the beginning of this section our object is to accelerate convergence to steady state. The calculation was run at a Courant number of 0.75. We show in Fig. 9 B_z near $y = d$ and observe a very quick approach to steady state $\sim 2 - 3\tau_c$. For $t > 0.6$ nsec we set $\alpha_E = \alpha_B = 0$ and revert back to the basic leapfrog scheme to show that one indeed has obtained steady state. In Fig. 10 we show B_z at $y = 0.5$ cm for the pure leapfrog algorithm. One observes the typical grid noise and what seems to be a slowly divergent trend. In Fig. 11, we show emission current as a function of time for both algorithms: diffusive and leapfrog. We note that the current density obtained by the leapfrog method oscillates around the steady-state value for the

[1] With this large value of the diffusivity, stability considerations make it necessary to use an implicit algorithm for the diffusion term in each equation.

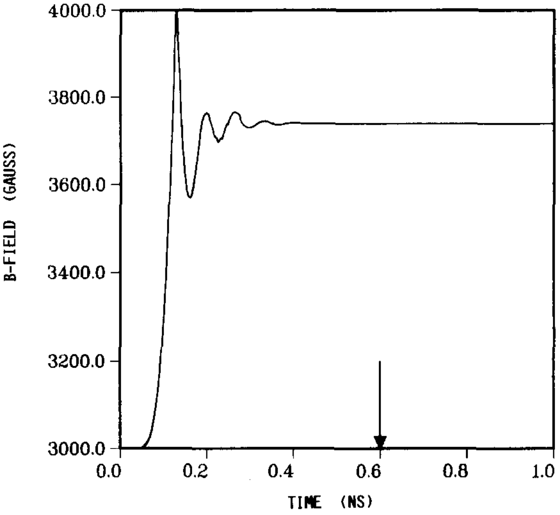

FIG. 9. *B* field at anode. Magnetic field at the anode as a function of time for the one-dimensional diode. The arrow indicates the change at $t = 0.6$ ns from the diffusive algorithm to leapfrog.

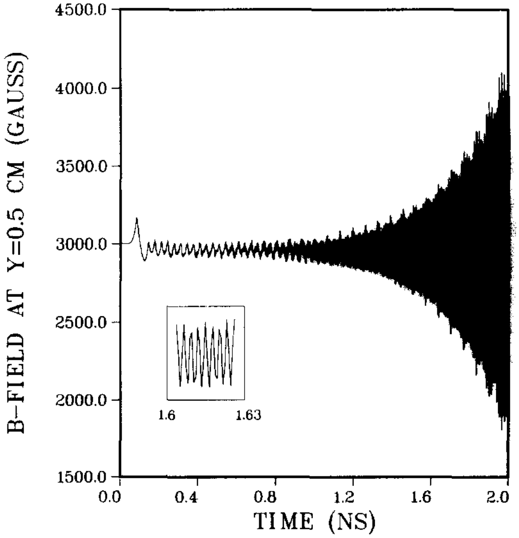

FIG. 10. Magnetic field at mid-gap as a function of time for leapfrog. Note apparent divergence of grid noise. Insert is a blow-up of plot for $1.6 < t < 1.63$ ns to show that the noise has the grid frequency ($\Delta t = 0.001$ ns).

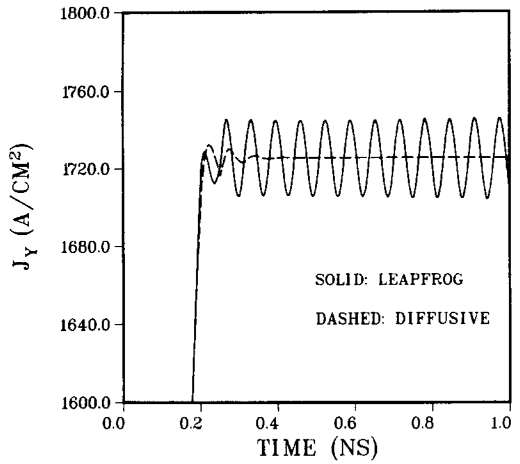

FIG. 11. Emission current density. Electron cathode emission current as a function of time for both algorithms used. See text for explanation; Leapfrog (—), diffusive (---).

current density obtained by using the diffusive algorithm. That steady-state value agrees with the analytic value(s) to within ~3 percent [6].

This result should be interpreted as an illustration of the technique we are using. We are aware that one could obtain for this simple case comparable results without considering the transverse part of the *E* & *M* fields using relaxation techniques, and/or by more sophisticated particle pushing and sharing algorithms.

SUMMARY AND CONCLUSION

We have adapted a technique used to suppress noise in the numerical solution of the equations of hydrodynamics to Maxwell's equations. The technique preserves the transverse longitudinal decomposition of the em fields and it is dissipative at short wavelengths. In the one- and two-dimensional vacuum em wave propagation it significantly reduced the computational errors with respect to the analytically known solutions over the leapfrog algorithm. This is true in the L_1, L_2, and L_∞ norms.

We have shown how a form of the algorithm, in which the numerical diffusion is always applied, was used to accelerate convergence to steady state in a case in which particle motion is coupled with the fields. At present we are developing a code for $2\frac{1}{2}$–D relativistic particle pushing em simulations, both for steady and time-dependent states, in which these ideas are used.

It remains to asses how important in different problems is the energy dissipation introduced by FRAM and to find plasma simulation cases in which its application demonstrably and significantly improves the accuracy of the results.

ACKNOWLEDGMENTS

The authors would like to express their sincere thanks to Drs. A Wilson and D. E. Parks for many useful discussions during the course of this work, and to Mr. P. G. Steen who developed the program used in the 1–D diode calculations. This work was supported by the U.S. Department of Energy under Contract DE-AC04-81AL16865, and the Defense Nuclear Agency under Contract DNA001-82-C-0078.

REFERENCES

1. M. CHAPMAN, *J. Comput. Phys.* **44** (1981).
2. J. P. BORIS, *in* "Proceedings of the Fourth Conference on the Numerical Simulation of Plasmas" (J. P. Boris and R. A. Shanny, Eds.), Office of Naval Research, Arlington, Va., p. 3, 1971; and references therein.
3. Note that this reduces the algorithm to be locally first order in space and time which is known to be a general consequence of requiring monotonicity in the numerical solution of hyperbolic differential equations. S. K. GODUNOV, *Mat. Sb.* **47** (1959), 271.
4. A. HARTEN, P. D. LAX, AND B. VAN LEER, *Siam Rev.* **25** (1983), 35.
5. R. V. LOVELACE AND E. OTT, *Phys. Fluids* **17** (1974), 1263; E. OTT AND R. V. LOVELACE, *Appl. Phys. Lett.* **27** (1975), 378; and references therein.
6. E. WAISMAN, *Appl. Phys. Lett.* **39** (1981), 447.